56 Gb/s Germanium Waveguide Electro-Absorption Modulator

Srinivasan Ashwyn Srinivasan, Marianna Pantouvaki, Shashank Gupta, Hong Tao Chen, Peter Verheyen, Guy Lepage, Gunther Roelkens, Krishna Saraswat, Dries Van Thourhout, Philippe Absil, and Joris Van Campenhout

(Top-Scoring Paper)

***Abstract*—We report a Germanium waveguide electro-absorption modulator with electro-optic bandwidth substantially beyond 50 GHz. The device is implemented in a fully integrated Si photonics platform on 200 mm silicon-on-insulator wafers with 220 nm top Si thickness. Wide open eye diagrams are demonstrated at 1610 nm operation wavelength for nonreturn-to-zero on-off keying (NRZ-OOK) modulation at data rates as high as 56 Gb/s. Dynamic extinction ratios up to 3.3 dB are obtained by applying drive voltages of 2 V peak-to-peak, along with an optical insertion loss below 5.5 dB. The device has a low junction capacitance of just 12.8 fF, resulting in 12.8 fJ/bit of dynamic and ~1.2 mW of static power consumption in typical operating conditions. Wafer-scale performance data are presented and confirm the manufacturability of the device. The demonstrated modulator shows great potential for realizing high-density and low-power silicon photonic transceivers targeting short-reach optical interconnects at serial data rates of 56 Gb/s and beyond.**

***Index Terms*—Electro-absorption modulators, optoelectronics, optical interconnects, waveguide modulators.**

I. Introduction

OPTICAL transceivers based on silicon (Si) photonics are increasingly being considered for short-reach interconnects in datacenters and for chip-to-chip interconnect applications [1]. Integrated Si photonics exploits the CMOS infrastructure to manufacture optical circuits, realizing cost benefits through economies of scale. Significant research and development have resulted in the demonstration of basic building blocks such as high-speed photodetectors [2], [3], modulators [4]–[13] and wavelength-division multiplexing filters [14] both in bulk CMOS [15], [16] and in SOI [17]–[21]. Among these components, modulators exploiting the free carrier dispersion effect in Si have been demonstrated in Mach–Zehnder interferometer (MZI) and ring resonator configurations. Si based MZI modulators have wide optical bandwidth suitable for high speed modulation but suffer from large footprints and relatively high power consumption [12]. On the contrary, ring based modulators in Si have small footprint and low power consumption but suffer from low optical bandwidth and are not robust against process and thermal variations [13]. Alternatively, electro-absorption modulators (EAM) exploit the Franz–Keldysh (FK) effect or the quantum-confined stark effect in epitaxially grown GeSi or Ge [4]–[10]. The FK effect is known to be a sub-picosecond phenomenon enabling high-speed modulation, and as such can be considered as a potential candidate to meet low energy-high bandwidth targets for Si based modulators [22], [23]. GeSi based EAMs have higher optical bandwidth than Si based ring modulators and lower footprint and power consumption than the Mach–Zehnder based modulators [7].

In this paper, we present wafer-scale data of a 56 Gb/s capable Ge waveguide EAM implemented in a sub-micron Si photonics platform using a 130 nm CMOS toolset. The demonstrated EAM has an insertion loss (IL) of 4.8 dB and dc extinction ratio (ER) of 4.6 dB at 1615 nm for a voltage swing of 2 Vpp, resulting in a minimum transmitter penalty (TP) of 9.1 dB. The device has a 3 dB bandwidth beyond 50 GHz and a junction capacitance of 12.8 fF for −1 V bias voltage. Clear open eye diagrams are demonstrated at a data rate of 56 Gb/s at 1610 nm with a dynamic ER of 3.3 dB for voltage swing of 2 Vpp. For non-return-to-zero on-off keying (NRZ-OOK) data rates of 56 Gb/s, the device consumes 12.8 fJ/bit of dynamic power at 2 Vpp voltage swing and 1.2 mW of static power due to light-current in typical peak-to-peak operating conditions.

II. Ge EAM: Design and Fabrication

The presented Ge EAM is designed to exploit the FK effect, which enables the modulation of the absorption coefficient of bulk Ge by an applied electric field for photon energies near the direct band gap of Ge [7]. An electric field difference of 50 kV/cm between the OFF and ON states can change the absorption coefficient in Ge by a factor of 3 [10]. Such strong electric field contrast between the two transmission states can

Manuscript received June 5, 2015; revised July 24, 2015; accepted August 25, 2015. Date of publication September 13, 2015; date of current version February 5, 2016. This work was supported by imec's industry-affiliation program on Optical I/O.

S. A. Srinivasan and H. T. Chen are with the Silicon Photonics Group, Interuniversity Microelectronics Center, Leuven B-3001, Belgium, the Photonics Research Group, Department of Information Technology, Ghent University-imec, and also with the Center for Nano- and Biophotonics, Ghent University, Ghent 9000, Belgium (e-mail: Ashwyn.Srinivasan@imec.be; Hongtao.Chen@imec.be).

M. Pantouvaki, P. Verheyen, G. Lepage, P. Absil, and J. Van Campenhout are with the Silicon Photonics Group, Interuniversity Microelectronics Center, Leuven B-3001, Belgium (e-mail: Marianna.Pantouvaki@imec.be; Peter.Verheyen@imec.be; Guy.Lepage@imec.be; Philippe.Absil@imec.be; Joris.VanCampenhout@imec.be).

D. Van Thourhout and G. Roelkens are with Photonics Research Group, Department of Information Technology, Ghent University-imec, and also with the Center for Nano- and Biophotonics, Ghent University, Ghent 9000, Belgium (e-mail: Dries.VanThourhout@intec.ugent.be; Gunther.Roelkens@intec.ugent.be).

S. Gupta and K. Saraswat are with Department of Electrical Engineering, Stanford University, Stanford, CA 94305 USA (e-mail: sgupta14@stanford.edu; saraswat@stanford.edu).

Color versions of one or more of the figures in this paper are available online at http://ieeexplore.ieee.org.

Digital Object Identifier 10.1109/JLT.2015.2478601

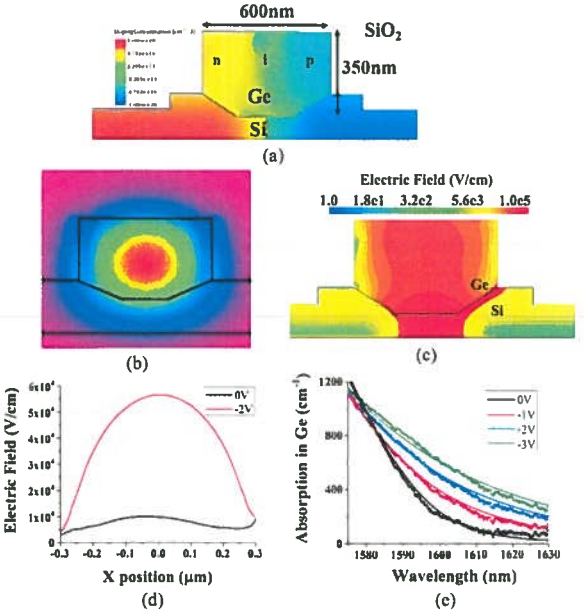

Fig. 1. (a) Cross-sectional schematic of the Ge EAM device integrated on a 220 nm SOI platform. (b) Optical field distribution in the 0.6 μm Ge waveguide. (c) Electric field distribution at –2 V. (d) Extracted electric field distribution at the center of the waveguide at 0 V and –2 V. (e) Simulated (solid-line) and measured (symbols) absorption coefficient of the Ge waveguide from [4].

be implemented using a p-i-n diode operated in reverse bias. In our Ge EAM design, we have adopted a lateral p-i-n diode, contacted from highly doped Si layers as shown in cross-section schematic in Fig. 1(a). The doping profile and doping level were optimized through electro-optic simulations using Sentaurus and RSOFT. A strong optical mode overlap with the electric field and sufficiently low free-carrier absorption due to dopants was obtained [see Fig. 1(a), Fig. 1(b) and Fig. 1(c)]. As shown in Fig. 1 (d), the 600 nm wide Ge waveguide has an electric field up to 9.8 kV/cm at 0 V and 56 kV/cm at –2 V along the width of the width of the Ge waveguide at half height. By combining the simulated electric field distribution in the waveguide, optical mode distribution, doping profile and Ge absorption spectrum including the FK effect, the absorption in the Ge waveguide can be accurately modeled as shown in Fig. 1(e).

A set of modulators with Ge length varying in the range of 10-80 μm and width varying in the range of 0.4–1 μm were fabricated in imec's iSiPP25G Si photonics platform using a 130 nm CMOS toolset [17]. The modulators were fabricated on a 200 mm SOI wafer with 220 nm top Si layer on 2 μm thick buried oxide (BOX). Ge was selectively grown in 110 nm deep recessed Si region using reduced pressure chemical vapor deposition. The wafer was annealed to decrease the threading dislocation density and the Ge islands were planarised with chemical mechanical polishing to a final thickness of 350 nm. Ge was doped with ion implantation to form n-type and p-type regions. The dopants were activated by annealing at 550 °C. Due to the mismatch in thermal expansion coefficient between the Ge epitaxial layer and the Si substrate, the Ge EAM devices exhibit an estimated tensile strain of 0.2% shifting the bandgap from 0.8 eV (1550 nm) to 0.78eV (1580 nm) as also reported in [10] and [24]. The Ge waveguides are coupled to a Si waveguide using low-loss tapers implemented in the poly-Si layer of the iSiPP25G technology. Grating couplers for transverse electric (TE) polarization with peak-coupling wavelength of 1610 nm were used for fiber coupling to and from the chip.

III. Modulator Performance: Static Characteristics

A device with an active area of 0.6 μm × 40 μm has been found to show the best electro-optic performance for NRZ-OOK modulation among the realized devices [10]. In order to assess the optical transmission loss through the Ge waveguide at different reverse bias, the loss spectra of the Ge EAM devices were measured and normalized with the transmission spectrum of a neighboring reference Si waveguide. Fig. 2(a) and (b) show the measured IL spectrum from 1580 to 1630 nm for TE polarization at 25 and 40°C. The absorption of the TE polarized light in the modulator is dominated by the HH-Γ band gap of Ge located at 1580nm. The red-shift in the absorption spectrum with temperature as shown in Fig. 2(b) is due to bandgap narrowing with temperature and is extracted to be 0.78 nm/°C.

Fig. 3(a) shows the extracted IL and ER from the measured loss spectra in Fig. 2. For a 2 V swing, the IL is 4.6 dB and the ER is 4.3 dB at 1615 nm. The indirect band absorption and the residual FK absorption due to the 9.8 kV/cm electric field at 0 V are two main contributions to the IL. The extracted IL also includes the coupling loss from the poly-Si taper between the Si waveguide and the Ge modulator. Fig. 3(b) shows the IL and ER extracted from 20 devices across a 200 mm wafer. The ER at –2 V has a wafer mean value of 4.6 dB with a standard deviation of 0.4 dB. The IL has an average value of 4.9 dB with a standard deviation of 0.8 dB. This illustrates the wafer-scale manufacturability of the device.

The TP of a modulator can be used to assess the optical loss and operational wavelength range of the modulator. It is defined as $TP = (P_{out}(1) - P_{out}(0))/(2 \times P_{in})$ where $P_{out}(1)$ and $P_{out}(0)$ are the high and low level of output optical power from the modulator and P_{in} is the input optical power [7]. The wafer mean TP for 2 V swing is measured to be 9.1 dB with a standard deviation of 0.6 dB and has a 1 dB bandwidth of greater than 22 nm (1607.5 – 1630 nm) as shown in Fig. 4(a) and (b). The complete 1 dB optical bandwidth could not be measured as the tunable laser could only sweep up to 1630 nm. The current operation wavelength of 1615 nm can be shifted to 1550 nm with the incorporation of ~1% Si during Ge epitaxial growth [7].

Fig. 5(a) shows the *I–V* characteristics of the device with and without illumination. At –1 and –2 V and room temperature, the Ge/Si diodes have a dark current of 12.5 nA and 47 nA respectively, indicating high quality epitaxial Ge. The light current was measured by operating the tunable laser at the peak wavelength of the grating coupler and aligning the fiber from the laser to the input grating coupler for maximum photo-current. The responsivity of the Ge EAM was extracted by sweeping the input waveguide power and monitoring the photocurrent. A responsivity of 1.2 A/W was extracted at –2 V for 1610 nm wavelength as shown in Fig. 5(b).

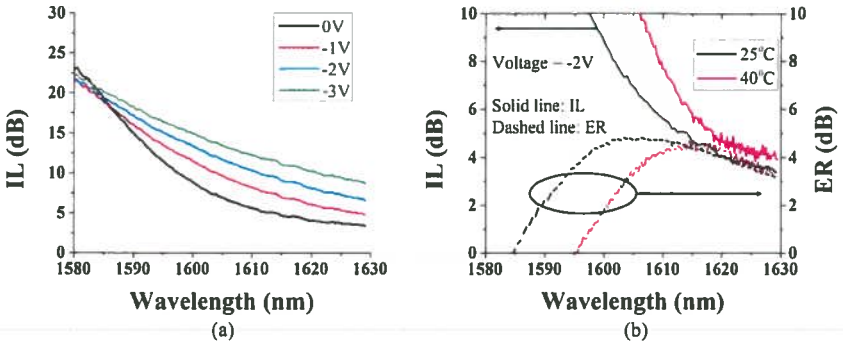

Fig. 2. (a) Extracted Insertion Loss (IL) spectrum through 0.6 μm wide and 40 μm long Ge waveguide at 0 V, –1 V, –2 V and –3 V at room temperature. (b) IL spectrum at 0 V and extracted Extinction Ratio (ER) spectrum at –2 V measured at 25 °C and 40 °C.

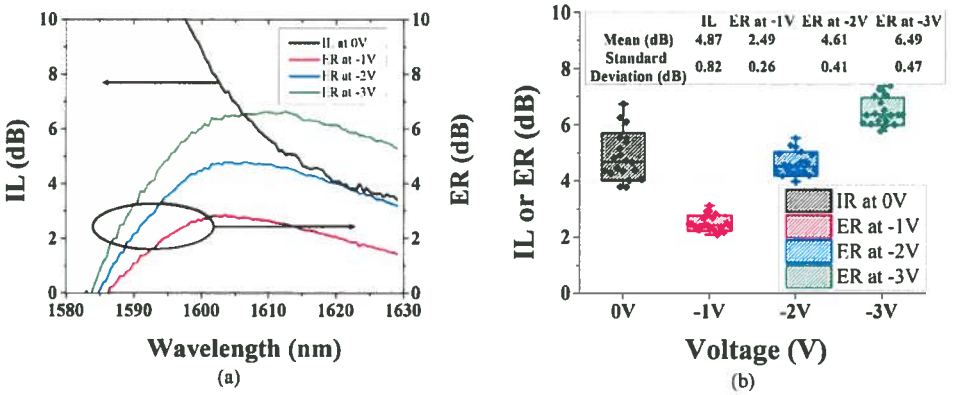

Fig. 3. (a) Extracted Insertion Loss (IL) and Extinction Ratio (ER) spectrum at –1 V, –2 V and –3 V. (b) IL and ER at 1615 nm across 20 devices located in a 200 mm SOI wafer. The box edge represents the standard deviation of the extracted data for each voltage.

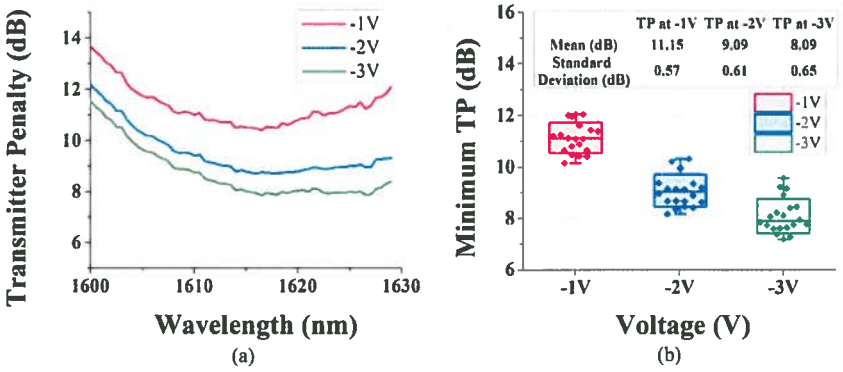

Fig. 4. (a) Transmitter penalty (TP) for different applied biases. (b) TP for 20 devices located in a 200 mm wafer.

IV. Modulator Performance: High-Speed Characteristics

The electro-optic bandwidth of the modulator was measured with a 50-GHz lightwave component analyzer. The RF system was calibrated to normalize the measurement with the RF response of the probe, cables, bias-tee and the photodetector. Fig. 6(a) shows typical S_{21} electro-optic S-parameter for various applied biases with an input optical power of 5 dBm. The 3 dB bandwidth of the modulator is greater than 50 GHz for –1 to –3 V. Since the FK effect is a phenomenon occurring on a sub-picosecond time scale [22], the speed of the modulator is limited by the RC delay. As the device is operated in reverse bias, higher reverse bias reduces the junction capacitance and increases its speed. This can be verified in Fig. 6(a) where the modulation bandwidth at –0.2 V is lower than at –1 V. The high-speed performance of the modulator can be further analyzed with the help of the equivalent circuit model in Fig. 6(b).

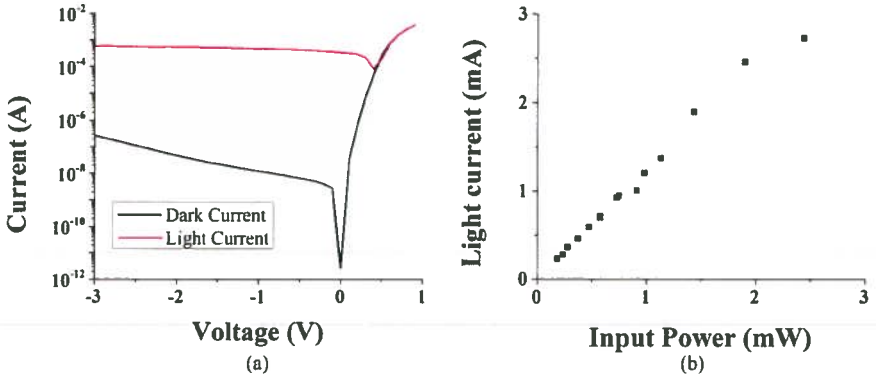

Fig. 5. (a) Measured I–V characteristics of the fabricated 0.6 × 40 μm Ge modulator. Light current was measured at 1610 nm with an input waveguide power of −3 dBm (0.5 mW). (b) Light current versus optical input optical power in the waveguide, showing a responsivity of 1.2 A/W at –2 V at 1615 nm.

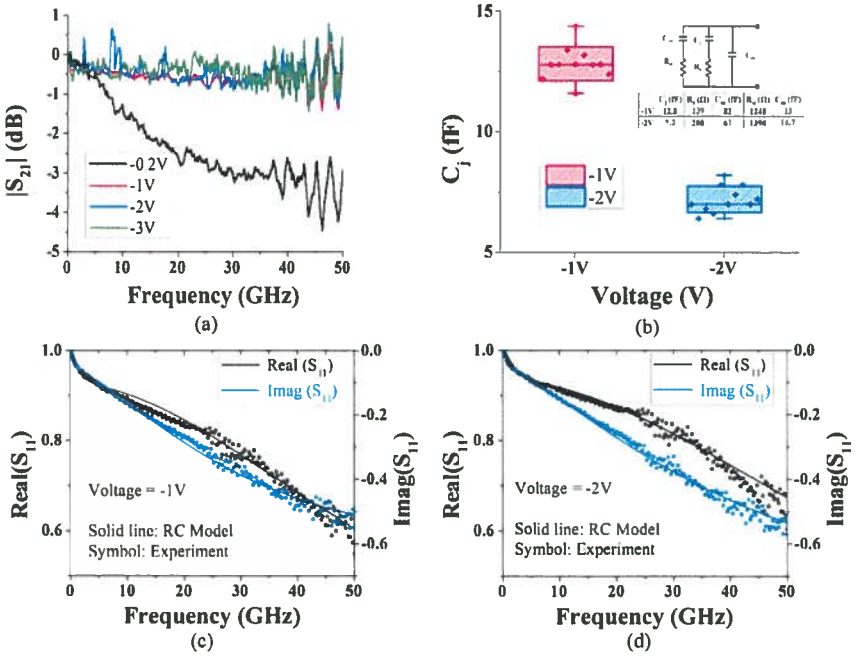

Fig. 6. (a) RF S_{21} measurements with a bandwidth >50 GHz at –0.2 V, –1 V, –2 V and –3 V with input power of 5 dBm. (b) Small signal equivalent circuit model of the modulator with extracted resistances and capacitances at –1 V and –2 V. (c) Fitting of the model with the RF S_{11} measurement at –1 V. (d) Fitting of the model with the RF S_{11} measurement at –2 V.

This model was used to fit the measured RF S_{11} parameter as shown in Fig. 4(b), Fig. 4(c) and Fig. 4(d) in order to extract the device's electrical parameters. R_s and C_j represent the reverse biased p-i-n junction, and R_{Si} and C_{ox} represent the current path through the Si substrate and the BOX, respectively. C_m represents the metal pad capacitance. On fitting the model to the S_{11} parameter across many devices, the extracted junction capacitance of the modulator is estimated to have a wafer mean of 12.8 and 7.2 fF at –1 and –2 V respectively, along with a series resistance of 138 and 280 Ω respectively suggesting a RC limited bandwidth beyond 80 GHz.

The large signal modulation of the modulator is shown in Fig. 7. A pseudorandom binary sequence (PRBS) signal with a pattern length of 2^{31}–1 and data rates of 28, 40 and 56 Gb/s generated with four 14 Gb/s MU181020B Anritsu pulse pattern generator and a MP1821A 50G/56 Gb/s MUX was delivered to the device with a 50 Ω terminated 50-GHz GS RF probe from Cascade Microtech. The modulated light was amplified using an L-band EDFA and filtered by an optical tunable filter with wavelength tunability of 1530-1610 nm, before reaching the oscilloscope. The measurements were performed with nominal peak-to-peak voltages of 1.5, 2.0 and 2.5 Vpp to modulate light at 1610 nm with input power of 0d Bm. The EDFA and the tunable filter limits the evaluation up to 1610 nm, which is 5 to 10 nm below the optimum wavelength with minimum TP. Clear and open eye diagrams with dynamic ER of 3.29 and 3.85 dB for 2 and 2.5 Vpp swing were obtained at 56 Gb/s with a signal-to-noise ratio greater than 5. To the best of our knowledge, this is the first demonstration of NRZ-OOK modulation at 56 Gb/s bit rates by a Ge EAM. Longer devices exhibit larger ER (~7dB

Fig. 7. Measured eye diagrams at room temperature at 1610 nm with 1.5 Vpp, 2.0 Vpp and 2.5 Vpp swing and with data rates of 28 Gb/s, 40 Gb/s and 56 Gb/s with input power of 0 dBm.

TABLE I
BENCHMARKING TABLE COMPARING THE PRESENTED GE EAM WITH OTHER TYPES OF STATE-OF-THE-ART SI, GESI AND GRAPHENE OPTICAL MODULATORS

Modulator Type	Ref.	Footprint	Wavelength	Voltage Swing	Optical Bandwidth	ER	IL	Power		3dB Bandwidth	Max. Bit Rate
								Static	Dynamic		
		[μm^2]	[nm]	[V]	[nm]	[dB]	[dB]	[mW]	[fJ/bit]	[GHz]	[Gb/s]
Si MZI	[6]	~3000×500	1300	1.5	>80	3.4	7.1	~20	~450	30	50
Si Ring	[13]	~10×10	1550	0.5	<0.1	6.4	1.2	<0.01	~1	21	44
III-V on Si	[4]	>100×350	1300	2.2	>30	>10	4.8	6.2	484	74	50
GeSi FK	[7]	~50×10	1550	3.0	>40	5.9	4.8	11.3	147	38	28
Ge FK	This work	**~40×10**	1615	**2.0**	>22.5	4.6	4.9	**1.2**	**12.8**	**>50**	**56**

at 2 Vpp) and can be used for higher order modulation formats such as PAM4, however at the expense of higher IL (~9dB) [10].

V. ESTIMATED POWER CONSUMPTION

The power consumption in an electro-optic modulator has two main contributions: dynamic power consumption and static power consumption [25]. The dynamic power consumption is defined as the amount of power required to switch the modulator from the ON to OFF state and vice versa. The junction capacitance extracted from the RF S_{11} parameter of the modulator can be used to estimate the average dynamic energy consumption per bit as $¼(C_j V_{pp}^2)$. With C_j = 12.8fF at bias voltage of –1 V, the dynamic energy consumption per bit is $¼(C_j V_{pp}^2)$ = 12.8fJ/bit for V_{pp} = 2 V. For a 56 Gb/s data transmission rate, the dynamic power consumption for 2 Vpp swing voltages is therefore 0.64 mW. The static power consumption in the EAM originates mostly from the light current and can be estimated as $½(P_{in}R_{on}V_{on}+P_{in}R_{off}V_{off})$. With a responsivity of 1.2 A/W at –2 V and input waveguide power of 0 dBm (1 mW) in typical operating conditions, the static power consumption is 1.2 mW. As a result, the total power consumption (dynamic and static) is 1.84 mW for 2 Vpp swing voltage at 56 Gb/s. Table I summarizes the key figures of merit comparing the presented Ge EAM with other Si, hybrid Si and Ge(Si) based modulators.

VI. CONCLUSION

We have demonstrated a 56 Gb/s Ge waveguide EAM integrated in a 220 nm SOI photonics platform. The modulator has a 3-dB bandwidth modulation greater than 50 GHz and a junction capacitance of 12.8 fF at –1 V. While operating at a data rate of 56 Gb/s, the device modulates light at 1610 nm with a dynamic ER of 3.29 dB. Due to ultralow capacitances, the total power consumption (dynamic and static) of the modulator is 1.84mW in typical operating conditions.

ACKNOWLEDGMENT

The authors acknowledge imec's 200 mm CMOS line for device fabrication and imec's PDK team for mask data preparation and tape out. Device layout was performed in IPKISS provided by Luceda Photonics.

REFERENCES

[1] D. A. B. Miller, "Device requirements for optical interconnects to silicon chips," *Proc. IEEE*, vol. 97, no. 7, pp. 1166–1185, Jul. 2009.

[2] C. T. DeRose, D. C. Trotter, W. A. Zortman, A. L. Starbuck, M. Fisher, M. R. Watts, and P. S. Davids, "Ultra compact 45 GHz CMOS compatible Germanium waveguide photodiode with low dark current," *Opt. Exp.* vol. 19, pp. 24897–24904, 2011.

[3] A. Novack, M. Gould, Y. Yang, Z. Xuan, M. Streshinsky, Y. Liu, G. Capellini, A. E.-J. Lim, G.-Q. Lo, T. Baehr-Jones, and M. Hochberg, "Germanium photodetector with 60 GHz bandwidth using inductive gain peaking," *Opt. Exp.* vol. 21, pp. 28387–28393, 2013.

[4] Y. Tang, J. D. Peters, and J. E. Bowers, "Over 67 GHz bandwidth hybrid silicon electroabsorption modulator with asymmetric segmented electrode for 1.3 μm transmission," *Opt. Exp.* vol. 20, pp. 11529–11535, 2012.

[5] Y. Tang, J. D. Peters, and J. E. Bowers, "Energy-efficient hybrid silicon electroabsorption modulator for 40-Gb/s 1-V uncooled operation," *IEEE Photon. Technol. Lett.*, vol. 24, no. 19, pp. 1689–1692, Oct. 1, 2012.

[6] M. Streshinsky, R. Ding, Y. Liu, A. Novack, Y. Yang, Y. Ma, X. Tu, E. K. Sing Chee, A. E.-J. Lim, P. G.-Q. Lo, T. Baehr-Jones, and M. Hochberg, "Low power 50 Gb/s silicon traveling wave Mach-Zehnder modulator near 1300 nm," *Opt. Exp.* vol. 21, pp. 30350–30357, 2013.

[7] D. Feng, W. Qian, H. Liang, C.-C. Kung, Z. Zhou; Z. Li, J. S. Levy, R. Shafiiha, J. Fong, B. J. Luff, and M. Asghari, "High-speed GeSi electroabsorption modulator on the SOI waveguide platform," *IEEE J. Sel. Topics Quantum Electron.*, vol. 19, no. 6, pp. 64–73, Nov./Dec. 2013.

[8] J. F. Liu, M. Beals, A. Pomerene, S. Bernardis, R. Sun, J. Cheng, L. C. Kimmerling, and J. Michel, "Waveguide- integrated, ultralow-energy GeSi electro-absorption modulators," *Nature Photon.*, vol. 2, no. 7, pp. 433–437, 2008.

[9] S. Ren, Y. Rong, S. A. Claussen, R. K. Schaevitz, T. I. Kamins, J. S. Harris, and D. A. B. Miller, "Ge/SiGe quantum well waveguide modulator monolithically integrated with SOI waveguides," *IEEE Photon. Technol. Lett.*, vol. 24, no. 6, pp. 461–463, Mar. 15, 2012.

[10] S. Gupta, S. A. Srinivasan, M. Pantouvaki, H. Chen, P. Verheyen, G. Lepage, D. V. Thourhout, G. Roelkens, K. Saraswat, P. Absil, and J. Van Campenhout, "50GHz Ge waveguide electro-absorption modulator integrated in a 220nm SOI photonics platform," presented at the *Optical Fiber Communication Confe.*, 2015, Paper Tu2A.4.

[11] M. Pantouvaki, H. Yu, M. Rakowski, P. Christie, P. Verheyen, G. Lepage, N. van Hoovels, P. Absil, and J. van Campenhout, "Comparison of silicon ring modulators with interdigitated and lateral p-n junctions," *IEEE J. Sel. Topics Quantum Electron.*, vol. 19, no. 2, p. 7900308, Mar./Apr. 2013.

[12] Xi Xiao, H. Xu, X. Li, Z. Li, T. Chu, Y. Yu, and J. Yu, "High-speed, low-loss silicon Mach–Zehnder modulators with doping optimization," *Opt. Exp.* vol. 21, pp. 4116–4125, 2013.

[13] E. Timurdogan, C. M. Sorace-Agaskar, J. Sun, E. S. Hossieni, A. Biberman, and M. R. Watts, "An ultralow power athermal silicon modulator," *Nature Commun.*, vol. 5, pp. 4008-1–4008-11, 2014.

[14] P. D. Heyn, J. D. Coster, P. Verheyen, G. Lepage, M. Pantouvaki, P. Absil, W. Bogaerts, J. van Campenhout, and D. van Thourhout, "Fabrication-tolerant four-channel wavelength-division-multiplexing filter based on collectively tuned si microrings," *J. Lightw. Technol.*, vol. 31, no. 16, pp. 2785–2792, Aug. 15, 2013.

[15] C. Sun, M. Georgas, J. Orcutt, B. Moss, Y.-H. Chen, J. Shainline, M. Wade, K. Mehta, K. Nammari, E. Timurdogan, D. Miller, O. Tehar-Zahav, Z. Sternberg, J. Leu, J. Chong, R. Bafrali, G. Sandhu, M. Watts, R. Meade, M. Popović, R. Ram, and V. Stojanović, "A monolithically-integrated chip-to-chip optical link in bulk CMOS," *IEEE J. Solid-State Circuits*, vol. 50, no. 4, pp. 828–844, Apr. 2015.

[16] P. Chaisakul, D. Marris-morini, J. Frigerio, D. Chrastina, M. Rouifed, S. Cecchi, and L. Vivien, "Integrated germanium optical interconnects on silicon substrates," *Nature Photon.*, vol. 8, no. 6, pp. 482–488, 2014.

[17] P. P. Absil, P. Verheyen, P. de Heyn, M. Pantouvaki, G. Lepage, J. de Coster, and J. van Campenhout, "Silicon photonics integrated circuits: A manufacturing platform for high density, low power optical I/O's," *Opt. Exp.*, vol. 23, pp. 9369–9378, 2015.

[18] M. Rakowski, M. Pantouvaki, P. de Heyn, P. Verheyen, M. Ingels, H. Chen, J. De Coster, G. Lepage, B. Snyder, K. de Meyer, M. Steyaert, N. Pavarelli, J. Su Lee, P. O'Brien, P. Absil, and J. van Campenhout, "22.5 A 4×20Gb/s WDM ring-based hybrid CMOS silicon photonics transceiver," in *Proc. IEEE Int. Solid- State Circuits Conf.*, Feb. 22–26, 2015, pp. 1–3.

[19] D. M. Gill, J.E. Proesel, C. Xiong, J. S. Orcutt, J. C. Rosenberg, M.H. Khater, T. Barwicz, S. Assefa, S. M. Shank, C. Reinholm, J. Ellis-Monaghan, E. Kiewra, S. Kamlapurkar, C. M. Breslin, W. M. J. Green, W. Haensch, and Y. A Vlasov, "Demonstration of a high extinction ratio monolithic CMOS integrated nanophotonic transmitter and 16 Gb/s Optical Link," *IEEE J. Sel. Topics Quantum Electron.*, vol. 21, no. 4, pp. 1–11, Jul./Aug. 2015.

[20] T. Baehr-Jones, R. Ding, A. Ayazi, T. Pinguet, M. Streshinsky, N. Harris, J. Li, L. He, M. Gould, Y. Zhang, A. Eu-Jin Lim, T.-Y. Liow, S. Hwee-Gee Teo, G.-Q. Lo, and M. Hochberg, "A 25 Gb/s silicon photonics platform," *arXiv:1203.0767v1*, Mar. 2012.

[21] M. Georgas, B. R. Moss, C. Sun, J. Shainline, J. S. Orcutt, M. Wade, Y.-H. Chen, K. Nammari, J. C. Leu, A. Srinivasan, R. J. Ram, M. A. Popovic, and V. Stojanović, "A monolithically-integrated optical transmitter and receiver in a zero-change 45nm SOI process," in *Proc. Symp. VLSI Circuits Digest Technical Papers*, Jun. 10–13, 2014, pp. 1–2.

[22] J. F. Lampin, L. Desplanque, and F. Mollot, "Detection of picosecond electrical pulses using the intrinsic Franz–Keldysh effect," *Appl. Phys. Lett.*, vol. 78, pp. 4103–4105, 2001.

[23] D. A. B. Miller, D. S. Chemla, and S. Schmitt-Rink, "Relation between electroabsorption in bulk semiconductors and in quantum wells: The quantum-confined Franz-Keldysh effect," *Phys. Rev. B*, vol. 33, pp. 6976–6982, 1986.

[24] Y. Ishikawa, K. Wada, J. Liu, D. D. Cannon, H.-C. Luan, J. Michel, and L. C. Kimerling, "Strain-induced enhancement of near-infrared absorption in Ge epitaxial layers grown on Si substrate," *J. Appl. Phys.*, vol. 98, pp. 013501-1–013501-9, 2005.

[25] D. A. B. Miller, "Energy consumption in optical modulators for interconnects," *Opt. Exp.*, vol. 20, pp. A293–A308, 2012.

Authors' biographies not available at the time of publication.